Phonon networks with SiV centers in diamond waveguides

M.-A. Lemonde[1], S. Meesala[2], A. Sipahigil[3,4], M. J. A. Schuetz[4], M. D. Lukin[4], M. Loncar[2], P. Rabl[1]
[1] *Vienna Center for Quantum Science and Technology, Atominstitut, TU Wien, 1040 Vienna, Austria*
[2] *John A. Paulson School of Engineering and Applied Sciences, Harvard University, 29 Oxford Street, Cambridge, MA 02138, USA*
[3] *Institute for Quantum Information and Matter and Thomas J. Watson, Sr., Laboratory of Applied Physics, California Institute of Technology, Pasadena, California 91125, USA and*
[4] *Department of Physics, Harvard University, Cambridge, Massachusetts 02138, USA*
(Dated: January 5, 2018)

We propose and analyze a novel realization of a solid-state quantum network, where separated silicon-vacancy centers are coupled via the phonon modes of a quasi-1D diamond waveguide. In our approach, quantum states encoded in long-lived electronic spin states can be converted into propagating phonon wavepackets and be reabsorbed efficiently by a distant defect center. Our analysis shows that under realistic conditions, this approach enables the implementation of high-fidelity, scalable quantum communication protocols within chip-scale spin-qubit networks. Apart from quantum information processing, this setup constitutes a novel waveguide QED platform, where strong-coupling effects between solid-state defects and individual propagating phonons can be explored at the quantum level.

Electronic and nuclear spins associated with defects in solids comprise a promising platform for the realization of practical quantum technologies [1]. A prominent example is the nitrogen-vacancy (NV) center in diamond [2, 3], for which techniques for state detection [4], coherent manipulations [5–7] and local entanglement operations [8–10] have been demonstrated and employed, for example, for various nanoscale sensing applications [11]. Despite this progress in the local control of spin qubits, integrating many spins into larger networks remains a challenging task. To achieve this goal, several schemes for interfacing spins via mechanical degrees of freedom have recently been discussed [12–17] and first experiments demonstrating magnetic [18–20] or strain-induced [21–25] couplings of mechanical vibrations to both long-lived spin states and electronic excited states of NV centers have been carried out. However, the weak intrinsic coupling of spins to vibrational modes and the short coherence of optically excited states make the extension of these methods into the quantum regime challenging.

In this Letter we describe the implementation of a phonon quantum network, where negatively-charged silicon-vacancy (SiV) centers are coupled via propagating phonon modes of a 1D diamond waveguide [26–29]. The electronic ground state of the SiV center features both spin and orbital degrees of freedom [30–32], which makes it naturally suited for this task; quantum states can be encoded in long-lived superpositions of the two lowest spin-orbit-coupled states [33–37], while a controlled admixing of higher orbital states, which are susceptible to strain, gives rise to a strong and tunable coupling to phonons. The central phonon frequency of $\sim$ 46 GHz set by the large spin-orbit splitting enables quantum-coherent operations already at convenient temperatures of $T \lesssim 1$ K, when thermal excitations at this frequency are frozen out. Our analysis shows that high-fidelity quantum state transfer protocols between distant SiV centers can be implemented under realistic conditions. Moreover, we propose a scalable operation of such phonon networks using switchable single-defect mirrors.

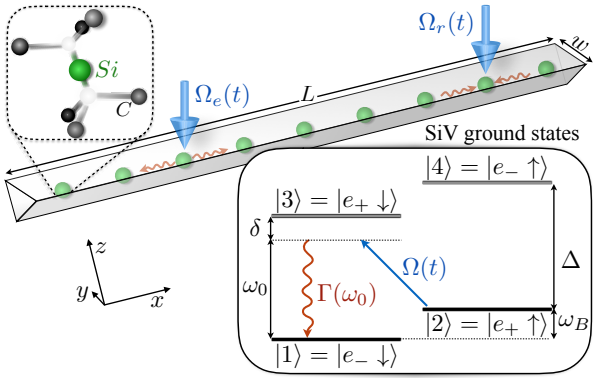

FIG. 1: Setup. An array of SiV defects is embedded in a 1D phonon waveguide. The inset shows the level structure of the electronic ground state of the SiV center. A tunable Raman process involving the excited state $|3\rangle$ is used to coherently convert the population of the stable state $|2\rangle$ into a propagating phonon, which can be reabsorbed by any other selected center along the waveguide. See text for more details.

Model.—We consider a system as depicted in Fig. 1, where an array of SiV centers is embedded in a 1D diamond waveguide. The electronic ground state of the SiV center is formed by an unpaired hole of spin $S = 1/2$, which occupies one of the two degenerate orbital states $|e_x\rangle$ and $|e_y\rangle$. In the presence of spin-orbit interactions and a weak Jahn-Teller effect, the four states are split into two doublets, $\{|1\rangle \simeq |e_-,\downarrow\rangle, |2\rangle \simeq |e_+,\uparrow\rangle\}$ and $\{|3\rangle \simeq |e_+,\downarrow\rangle, |4\rangle \simeq |e_-,\uparrow\rangle\}$, which are separated by $\Delta/2\pi \simeq 46$ GHz [31, 32]. Here, $|e_\pm\rangle = (|e_x\rangle \pm i|e_y\rangle)/\sqrt{2}$ are eigenstates of the orbital angular momentum operator, i.e. $L_z|e_\pm\rangle = \pm\hbar|e_\pm\rangle$, where the z-axis is along the symmetry axis of the defect. In the presence of a mag-

netic field $\vec{B} = B_0\vec{e}_z$, the Hamilton operator for a single SiV center is ($\hbar = 1$)

$$H_{\rm SiV} = \omega_B|2\rangle\langle 2| + \Delta|3\rangle\langle 3| + (\Delta+\omega_B)|4\rangle\langle 4| + \frac{1}{2}\left[\Omega(t)e^{i[\omega_d t+\theta(t)]}\left(|2\rangle\langle 3| + |1\rangle\langle 4|\right) + \text{H.c.}\right], \quad (1)$$

where $\omega_B = \gamma_s B_0$ and γ_s is the spin gyromagnetic ratio. In Eq. (1), we have included a time-dependent driving field with a tunable Rabi-frequency $\Omega(t)$ and phase $\theta(t)$, which couples the lower and upper states of opposite spin. This coupling can be implemented either directly with a microwave field of frequency $\omega_d \sim \Delta$ [38], or indirectly via an equivalent optical Raman process [39]. The latter method is already used in experiments to initialize and prepare individual SiV centers in superpositions of $|1\rangle$ and $|2\rangle$ [33–35] with coherence times that can exceed 10 ms in the absence of thermal processes and with dynamical decoupling [36]. Further details on the derivation of $H_{\rm SiV}$ are given in the supplementary material [39].

For the waveguide, we consider a quasi-1D geometry of width w and length $L \gg w$. The waveguide supports travelling phonon modes of frequency $\omega_{n,k}$ and mode function $\vec{u}_{n,k}(\vec{r}) \sim \vec{u}^{\perp}_{n,k}(y,z)e^{ikx}$, where k is the wavevector along the waveguide direction, n is the branch index and $\vec{u}^{\perp}_{n,k}(y,z)$ is the transverse profile of the displacement field. The phonons induce transitions between the orbital states $|e_\pm\rangle$ [40–42], and the Hamiltonian for the whole system reads

$$H = \sum_j H^{(j)}_{\rm SiV} + \sum_{n,k}\omega_{n,k}a^\dagger_{n,k}a_{n,k} + \frac{1}{\sqrt{L}}\sum_{j,k,n}\left(g^j_{n,k}J^j_+ a_{n,k}e^{ikx_j} + \text{H.c.}\right). \quad (2)$$

Here j labels the SiV centers located at positions $\vec{r}_j = (x_j, y_j, z_j)$, $J_- = (J_+)^\dagger = |1\rangle\langle 3| + |2\rangle\langle 4|$ is the spin-conserving lowering operator and $a_{n,k}$ ($a^\dagger_{n,k}$) are the annihilation (creation) operators for the phonon modes. The couplings $g^j_{n,k} \equiv g_{n,k}(y_j, z_j)$ depend on the components of the local strain tensor, $\epsilon^{ab}_{n,k}(\vec{r}_j) = \frac{1}{2}[\frac{\partial}{\partial x_b}u^a_{n,k}(\vec{r}_j) + \frac{\partial}{\partial x_a}u^b_{n,k}(\vec{r}_j)]$, and can be evaluated for a known transverse mode profile $\vec{u}^{\perp}_n(y,z)$ [39, 42]. We express the resulting couplings as

$$g^j_{n,k} = d\sqrt{\frac{\hbar k^2}{2\rho A\omega_{n,k}}}\xi_{n,k}(y_j, z_j), \quad (3)$$

where $d/2\pi \sim 1$ PHz is the strain sensitivity of the orbital states [40, 41], ρ the density and A the transverse area of the waveguide. The dimensionless coupling profile $\xi_{n,k}(y,z)$ accounts for the specific strain distribution and $\xi(y,z) = 1$ for a homogeneous compression mode.

From cavity to waveguide QED.—For small structures, $L \sim 10 - 100\,\mu$m, $w \lesssim 200$ nm, and group velocities

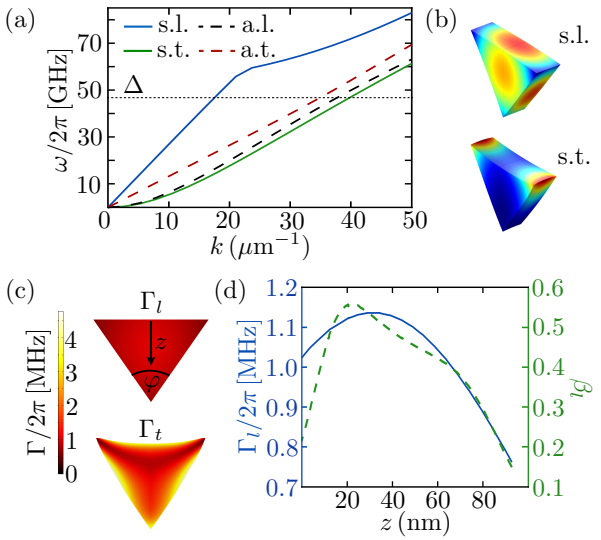

FIG. 2: Phonon waveguide. (a) Acoustic dispersion relation for a triangular waveguide of width $w = 130$ nm and etch-angle $\varphi = 35^o$. Symmetric (solid lines) and anti-symmetric (dashed lines) branches with respect to the vertical mirror-symmetry plane are shown. (b) Normalized displacement profiles of the symmetric phonons at 46 GHz. (c) The emission rates into the symmetric longitudinal (Γ_l) and transverse (Γ_t) polarization modes at 46 GHz are plotted for different positions of the SiV center within the triangular cross-section. (d) Γ_l and fraction (β_l) of spontaneous emission into the longitudinal branch for different positions of the SiV center along the vertical mirror-symmetry axis. For all results, an orientation of the waveguide along the [110] crystal axis of diamond and SiV centers oriented along $[\bar{1}11]$ and $[1\bar{1}1]$, i.e., orthogonal to the waveguide axis, have been assumed.

$v \sim 10^4$ m/s, the individual phonon modes are well separated in frequency, $\Delta\omega/2\pi \gtrsim 50$ MHz, and the SiV centers can be coupled to a single standing-wave mode with a strength $g_L = g_0\sqrt{\lambda/L} \approx 2\pi \times (4-14)$ MHz, where $g_0/2\pi \approx 105$ MHz and $\lambda \approx 200$ nm is the phonon wavelength. The system dynamics is then governed by a Jaynes-Cummings-type interaction between phonons and orbital states [39]. In the strong coupling regime, $g_L > \kappa = \Delta/Q$, which is reached for moderate mechanical quality factors of $Q > 10^4$, a coherent exchange of phonons and defect excitations becomes possible. For longer waveguides, the coupling to the quasi-continuum of phonon modes is characterized by the resulting decay rate $\Gamma_j(\Delta) = \sum_n \Gamma_{j,n}(\Delta)$ for states $|3\rangle$ and $|4\rangle$, where

$$\Gamma_{j,n}(\omega) = \lim_{L\to\infty}\frac{2\pi}{L}\sum_k |g^j_{n,k}|^2\delta(\omega - \omega_{n,k}). \quad (4)$$

For a single compression mode with $\vec{u}^{\perp}(y,z) \sim \vec{x}$ and a linear dispersion $\omega_k = vk$, we obtain $\Gamma(\omega) = d^2\hbar\omega/(\rho A v^3)$, which results in a characteristic phonon emission rate of $\Gamma(\Delta)/2\pi \sim 1$ MHz [42].

Figure 2 summarizes the simulated acoustic dispersion relations and the resulting decay rates for a triangular

waveguide [26, 40] of width $w = 130$ nm. The SiV centers couple primarily to a longitudinal (l) compression and a transverse (t) flexural mode with group velocities $v_l = 1.71 \times 10^4$ m/s and $v_t = 0.73 \times 10^4$ m/s, respectively. The coupling to the other two branches of odd symmetry can be neglected for defects near the center of the waveguide. Fig. 2(c) and (d) show that the rates $\Gamma_{l,t}$ are quite insensitive to the exact location of the SiV center. However, the fraction of phonons emitted into a specific branch, $\beta_n = \Gamma_n/\Gamma$, is significantly below unity as emission is split between a pair of modes. In optical waveguides [43], a value of $\beta < 1$ usually arises from the emission of photons into non-guided modes, which are irreversibly lost. For a phonon waveguide this is not the case, but the multi-branch nature of the waveguide must be fully taken into account. In all examples below we assume $\beta_l = \beta_t = 0.5$, which is most relevant for SiV defects located near the center of the beam.

Coherent spin-phonon interface.—We are interested in the transfer of a qubit state, encoded into the stable states $|1\rangle$ and $|2\rangle$, between an arbitrary pair of emitting (e) and receiving (r) defects in the waveguide,

$$(\alpha|1\rangle_e + \beta|2\rangle_e)|1\rangle_r \to |1\rangle_e(\alpha|1\rangle_r + \beta|2\rangle_r). \qquad (5)$$

As shown in Fig. 1, this can be achieved by inducing a Raman transition via state $|3\rangle_e$ to convert the population in state $|2\rangle_e$ into a propagating phonon and by reverting the process at the receiving center. For low enough temperatures, $T \ll \hbar\Delta/k_B \approx 2.2$ K, such that all phonon modes are initially in the vacuum state, this scenario is described by the following ansatz for the wavefunction $|\psi(t)\rangle = [\alpha\mathbb{1} + \beta C^\dagger(t)]|\bar{1}, 0\rangle$, where $|\bar{1}, 0\rangle$ is the ground state with all SiV centers in state $|1\rangle$ and $C^\dagger(t) = \sum_{j=e,r}\left[c_j(t)e^{-i\omega_B t}|2\rangle_j\langle 1| + b_j(t)e^{-i\omega_0 t}|3\rangle_j\langle 1| + \sum_{n,k} c_{n,k}(t)e^{-i\omega_0 t}a^\dagger_{n,k}\right]$ creates a single excitation distributed between the SiV centers and the phonon modes. The central phonon frequency $\omega_0 = \Delta_j + \delta_j$ is assumed to be fixed by compensating small inhomogeneities in the Δ_j by the detunings $\delta_j = \omega_d^j - (\Delta_j - \omega_B^j)$.

By adiabatically eliminating the fast decaying amplitudes b_j, we derive effective equations of motion for the slowly varying amplitudes $c_i(t)$. From this derivation, detailed in [39], we obtain for each qubit amplitude

$$\dot{c}_j(t) = -\frac{\gamma_j(t)}{2}c_j(t) - \sum_n \sqrt{\frac{\gamma_{j,n}(t)}{2}}e^{-i\theta_j(t)}\Phi^{\rm in}_{j,n}(t), \quad (6)$$

where $\gamma_j(t) = \sum_n \gamma_{j,n}(t)$ is the effective decay rate of state $|2\rangle_j$ and

$$\gamma_{j,n}(t) = \frac{\Omega_j^2(t)}{4\delta_j^2 + \Gamma_j^2(\omega_0)}\Gamma_{j,n}(\omega_0). \qquad (7)$$

Assuming $0 \le \Omega(t)/2\pi < 70$ MHz and $\delta/2\pi = 100$ MHz, this rate can be tuned between $\gamma_j = 0$ and a maximal value of $\gamma_{\max}/2\pi \approx 250$ kHz, which is still fast compared to the expected bare dephasing times $T_2^* = 10 - 100\,\mu$s of the qubit state [36]. At the same time, the large detuning $\delta \gg \Gamma(\Delta)$ ensures that any residual scattering of phonons from an undriven defect is strongly suppressed [39].

The last term in Eq. (6), where $\Phi^{\rm in}_{j,n} = \Phi^{\rm in,L}_{j,n} + \Phi^{\rm in,R}_{j,n}$, describes the coupling of an SiV center to the left- (L) and right- (R) incoming fields $\Phi^{\rm in,R/L}_{j,n}$, which themselves are related to the corresponding outgoing fields by [44]

$$\Phi^{\rm out,R/L}_{j,n}(t) = \Phi^{\rm in,R/L}_{j,n}(t) + \sqrt{\frac{\gamma_{j,n}(t)}{2}}c_j(t)e^{i\theta_j(t)}. \qquad (8)$$

Together with Eq. (6), these input-output relations specify the local dynamics at each node and must be supplemented by a set of propagation relations for all fields [cf. Fig. 3(a)]. As an example, for $x_r > x_e$, the right propagating fields obey $\Phi^{\rm in,R}_{r,n}(t) = \Phi^{\rm out,R}_{e,n}(t - \tau^n_{er})e^{i\phi^n_{er}}$, where $\tau^n_{er} = (x_r - x_e)/v_n$ and $\phi^n_{er} = k_n(x_r - x_e)$ are the respective propagation times and phases. Reflections at the boundaries lead to a retarded interaction of each center with its own emitted field. For example, $\Phi^{\rm in,R}_{e,n}(t) = -\sqrt{R_n}\Phi^{\rm out,L}_{e,n}(t - \tau^n_e)e^{i\phi^n_e}$, where $\tau^n_e = 2x_e/v_n$ and $\phi^n_e = 2k_n x_e$, and the reflectivity $R_n \le 1$ has been introduced to model losses. The combined set of time-nonlocal equations for the SiV amplitudes can be solved numerically for given positions x_j and pulses $\gamma_{j,n}(t)$. Since any deterministic phase acquired during the protocol can be undone by a local qubit rotation, we identify $\mathcal{F}(t) = |c_r(t)|^2$ with the fidelity of the transfer, which exceeds the classical bound for $\mathcal{F} > 2/3$ [45].

Quantum state transfer.—In Fig. 3(b) we first consider constant rates $\gamma_{j,n}(t) = \gamma_{\max}/2$, in which case a state transfer is achieved over multiple round-trips of the emitted wave-packet. For $L \sim 100\,\mu$m, the round-trip times $2L/v_n$ are still short compared to $\gamma^{-1}_{\max}$ and we recover the standing-wave picture with splittings $\Delta\omega_n = \pi v_n/L$ between consecutive k-modes. When only the transverse mode is resonant, [i.e., $\phi^t_L = \phi^t_e + \phi^t_r + 2\phi^t_{er} = 2\pi n$, while $\phi^l_L = (2m+1)\pi$] and for maximal coupling [$\phi^l_e = \phi^l_r = (2m+1)\pi$], we observe damped oscillations with a fast frequency $\tilde{g} = \sqrt{\gamma_{\max}\Delta\omega_t/2\pi} \approx 2\pi \times 1.2$ MHz and decay rate $\kappa = -\frac{\Delta\omega}{\pi}\log R \approx 2\pi \times 0.93$ MHz. This result is expected from a single-mode description of the waveguide [39], and is recovered here as a limiting case of our general framework. The losses from multiple imperfect reflections at the boundaries can be partially suppressed at the expense of a slightly slower transfer by detuning the SiV centers from the closest mode by $\delta_0 > \tilde{g}$. In this case the SiV centers communicate via an exchange of virtual phonons and $\kappa \to \kappa(\tilde{g}/\delta_0)^2$. For a maximal detuning $\delta_0 = \Delta\omega_t/2$, the transfer fidelity scales approximately as $\mathcal{F} \simeq R - \pi^2/(8T_2^*\gamma_{\max})$ [39]. For $T_2^* \approx 100\mu$s and $R > 0.99$, which can be achieved, for example, by phononic Bragg mirrors [46], gate fidelities of $\mathcal{F} \gtrsim 0.99$ are possible.

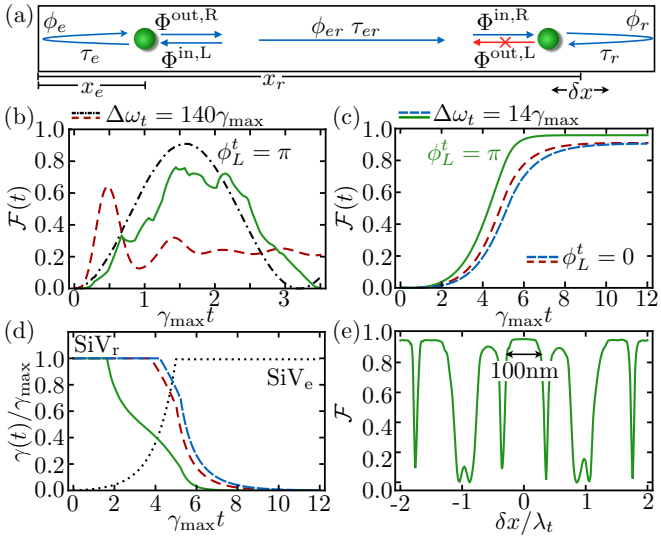

FIG. 3: State transfer protocol. (a) Schematics showing the relevant fields, retardation times and propagation phases. (b) State transfer fidelity for constant rates $\gamma_e(t) = \gamma_r(t) = \gamma_{\max}$. The case of a single resonant mode (red dashed line; $\phi_L^t = 0$, $\phi_L^l = \pi$) is compared to the off-resonant case (dot-dashed black line; $\phi_L^t = \phi_L^l = \pi$) for $L \sim 100\,\mu$m ($\Delta\omega_t/\gamma_{\max} = 140$). The full green line represents the long-waveguide counterpart of the off-resonant scenario, where $L \sim 1$ mm ($\Delta\omega/\gamma_{\max} = 14$). (c)-(d) Protocol using slowly-varying control pulses ($t_p\gamma_{\max} = 1$) where $\Phi_{r,t}^{\text{out,L}}(t)$ is completely suppressed. The dashed blue line corresponds to the long waveguide counter part of the dashed red line. For (b)-(d), the two defects are equally coupled to both modes, $\phi_e^n = \phi_r^n = \pi$ and $\beta_e^n = \beta_r^n = 0.5$. (e) Plot of the state transfer fidelity for varying positions of the receiving SiV center. For this plot $\phi_L^t = \phi_L^l = \pi$ and a maximal transfer time of $12\gamma_{\max}^{-1}$ have been assumed. In all plots, we considered defects near the boundaries where $\tau_e = \tau_r \approx 0$. To illustrate the effect of phonon losses a boundary reflectivity of $R = 0.92$ has been assumed, which corresponds to $Q \approx 5\times10^4$ in the cavity limit.

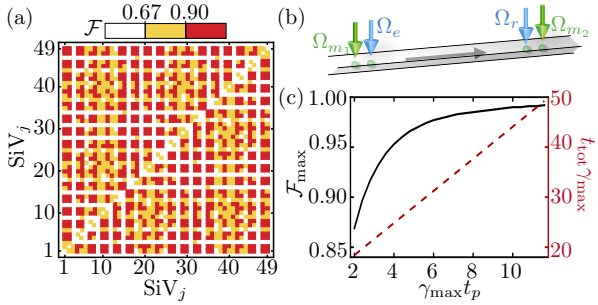

FIG. 4: Scalability. (a) Quantum connectivity matrix for 49 SiV centers equally spaced in a 500 μm long waveguide. The maximal protocol time is fixed to $12\gamma_{\max}^{-1}$ and $R = 0.92$. (b) State-transfer protocol in an infinite waveguide where the outermost SiV centers act as switchable mirrors. The full black line shows the fidelity as a function of the characteristic time of the emitting pulse, t_p, while the dashed red curve shows the total protocol time, t_{tot}. For the considered positions the propagation phases between each center and their neighboring mirror defect is π for both phonon branches and $\Delta\phi_{er} = 2\pi \times n$. In all simulations, a constant decay rate for the mirror defects, $\gamma_{m_1}(t) = \gamma_{m_2}(t) = \gamma_{\max}$, maximizes the fidelity.

As illustrated by the solid line in Fig. 3(b), the simple cavity picture fails for longer waveguides, where multimode and propagation effects become non-negligible. In Fig. 3(c) we illustrate a more general and more robust protocol, where the phonons ideally travel the waveguide only once. Here, the emission is gradually turned on with a fixed pulse $\gamma_e(t)/\gamma_{\max} = \min\{1, e^{(t-5t_p)/t_p}\}$, while $\gamma_r(t)$ and $\theta_r(t)$ are constructed numerically by minimizing at every time step the back-reflected transverse field $|\Phi_{r,t}^{\text{out,L}}|$. For slow pulses, $\gamma_{\max}t_p \gg 1$, a perfect destructive interference between the field reflected from the boundary and the field emitted by the receiving center can be achieved, i.e., $\Phi_{r,t}^{\text{in,L}}(t) + \sqrt{\gamma_{r,t}(t)/2}c_r(t)e^{i\theta_r(t)} = 0$. For a single branch ($\beta_t = 1$) this results in a complete suppression of the signal traveling back to the emitting center so that for $R = 1$ and negligible retardation effects, a perfect state transfer can be implemented [13, 47–49]. Fig. 3(c) shows that this approach also leads to high transfer fidelities under more general conditions, where all propagation effects are taken into account and multiple independent channels participate in the transfer. Importantly, since there are no resonances building up, this strategy is independent of L and can be applied for short and long waveguides equally well.

In the examples shown in Fig. 3(b)-(d), the SiV centers are placed at positions near the ends of the waveguide, where the effective emission rate $\tilde{\gamma}_{j,n}(t) = 2\gamma_{j,n}(t)\sin^2(\phi_j^n/2)$ [50] into both modes is maximal. Fig. 3(e) shows the achievable transfer fidelities when the position of the receiving center is varied over several wavelengths. We observe plateaus of high fidelity extending over $\sim$ 100 nm, interrupted by a few sharp dips arising from a complete destructive interference, i.e. $\phi_r \approx \pi$. This position insensitivity, even in a multichannel scenario, can be understood from a more detailed inspection of the outgoing fields $\Phi_{r,l}^{\text{out,L}}$ [39] and makes the transfer protocol consistent with uncertainties of $\delta x < 50$ nm achieved with state-of-the-art implantation techniques [51].

Scalability.—In Fig. 4 (a), we consider a waveguide of length $L = 500\,\mu$m containing 49 SiV centers spaced by $\Delta x = 10\,\mu$m to allow individual addressing by optical or microwave fields. The resulting quantum connectivity matrix, i.e. the achievable state transfer fidelity between each pair, shows that apart from a few exceptions, most centers can be connected efficiently and that in principle, the operation of large scale networks is possible. By using phononic bandstructure engineering [46, 52], single mode [53] or chiral phononic waveguides [54], the transfer fidelities can be further increased beyond the basic scenario considered here. In practice, propagation losses and elastic phonon scattering will set additional

limitations for the overall size of the network. In Fig. 4 (b), we show a general strategy to overcome these limitations by separating the whole waveguide into smaller segments using additional 'mirror centers'. Here the two outermost SiV centers simply reflect the incoming phonon wavepacket [55], and thus create an effective cavity within the waveguide [56, 57]. This is illustrated in Fig. 4 (b), where we plot the resulting state transfer fidelity for two SiV centers localized inside this effective cavity. For transfer pulses that are long compared to $\gamma_{\rm max}^{-1}$, the outmost centers act as almost perfect mirrors, such that even in an infinite waveguide state transfer protocols within reconfigurable sections of the network can be implemented.

Conclusion.—We have shown how an efficient coupling between individual SiV centers and propagating phonons in a diamond waveguide can be realized and used for quantum networking applications. By employing direct spin-phonon couplings in the presence of a transverse magnetic field [58] or defect-phonon interactions in other materials [59–61], many of the described techniques could also be adapted for lower phonon frequencies $\sim 5-10$ GHz, where many advanced phononic engineering methods are already available. When combined with local control operations involving adjacent nuclear spins as quantum memories [10, 33, 62, 63], the set of all these techniques provides a realistic approach for a scalable quantum information processing platform with spins in solids.

Acknowledgements.—This work was supported by the Austrian Science Fund (FWF) through the SFB FoQuS, Grant No. F40, the START Grant No. Y 591-N16, ONR MURI on Quantum Optomechanics (Award No. N00014-15-1-2761), STC Center for Integrated Quantum Materials (NSF Grant No. DMR-1231319), NSF EFRI ACQUIRE (Award No. 5710004174), CUA, NSF and Vannevar Bush Fellowship.

[1] T. D. Ladd, F. Jelezko, R. Laflamme, Y. Nakamura, C. Monroe, and J. L. O'Brien, Quantum computers, Nature (London) **464**, 7285 (2010).

[2] M. W. Doherty, N. B. Manson, P. Delaney, F. Jelezko, J. Wrachtrup, and L. C. L. Hollenberg, The nitrogen-vacancy colour centre in diamond, Phys. Rep. **528**, 1 (2013).

[3] L. Childress, R. Walsworth, and M. D. Lukin, Atom-like crystal defects, Phys. Today **67**, 38 (2014).

[4] F. Jelezko, T. Gaebel, I. Popa, A. Gruber, and J. Wrachtrup, Observation of coherent oscillations in a single electron spin, Phys. Rev. Lett. **92**, 076401 (2004).

[5] L. Childress, M.V. Gurudev Dutt, J. M. Taylor, A. S. Zibrov, F. Jelezko, J. Wrachtrup, P. R. Hemmer, and M. D. Lukin, Coherent Dynamics of Coupled Electron and Nuclear Spin Qubits in Diamond, Science **314**, 5797 (2006).

[6] G. de Lange, Z. H. Wang, D. Riste, V. V. Dobrovitski, and R. Hanson, Universal Dynamical Decoupling of a Single Solid-State Spin from a Spin Bath, Science **330**, 60 (2010).

[7] L. C. Bassett, F. J. Heremans, D. J. Christle, C. G. Yale, G. Burkard, B. B. Buckley, and D. D. Awschalom, Ultrafast optical control of orbital and spin dynamics in a solid-state defect, Science **345**, 6202 (2014).

[8] W. Pfaff, T. H. Taminiau, L. Robledo, H. Bernien, M. Markham, D. J. Twitchen, and R. Hanson, Demonstration of entanglement-by-measurement of solid-state qubits, Nat. Phys. **9**, 29 (2013).

[9] F. Dolde, I. Jakobi, B. Naydenov, N. Zhao, S. Pezzagna, C. Trautmann, J. Meijer, P. Neumann, F. Jelezko, and J. Wrachtrup, Room-temperature entanglement between single defect spins in diamond, Nat. Phys. **9**, 139 (2013).

[10] G. Waldherr, Y. Wang, S. Zaiser, M. Jamali, T. Schulte-Herbrüggen, H. Abe, T. Ohshima, J. Isoya, J. F. Du, P. Neumann, and J. Wrachtrup, Quantum error correction in a solid-state hybrid spin register, Nature (London) **506**, 204 (2014).

[11] L. Rondin, J.-P. Tetienne, T. Hingant, J.-F. Roch, P. Maletinsky, and V. Jacques, Magnetometry with nitrogen-vacancy defects in diamond, Rep. Prog. Phys. **77**, 056503 (2014).

[12] P. Rabl, S. J. Kolkowitz, F. H. Koppens, J. G. E. Harris, P. Zoller, and M. D. Lukin, A quantum spin transducer based on nanoelectromechanical resonator arrays, Nat. Phys. **6**, 602 (2010).

[13] S. J. M. Habraken, K. Stannigel, M. D. Lukin, P. Zoller, and P. Rabl, Continuous mode cooling and phonon routers for phononic quantum networks, New J. Phys. **14**, 115004 (2012).

[14] S. D. Bennett, N. Y. Yao, J. Otterbach, P. Zoller, P. Rabl, and M. D. Lukin, Phonon-Induced Spin-Spin Interactions in Diamond Nanostructures: Application to Spin Squeezing, Phys. Rev. Lett., **110**, 156402 (2013).

[15] A. Albrecht, A. Retzker, F. Jelezko, and M. B. Plenio, Coupling of nitrogen vacancy centres in nanodiamonds by means of phonons, New J. Phys. **15**, 083014 (2013).

[16] M. J. A. Schuetz, E. M. Kessler, G. Giedke, L. M. K. Vandersypen, M. D. Lukin, and J. I. Cirac, Universal Quantum Transducers Based on Surface Acoustic Waves, Phys. Rev. X **5**, 031031 (2015).

[17] D. Lee, K. W. Lee, J. V. Cady, P. Ovartchaiyapong and A. C. Bleszynski Jayich, Topical review: spins and mechanics in diamond, J. Opt. **19**, 033001 (2017).

[18] D. Rugar, R. Budakian, H. J. Mamin, and B. W. Chui, Single spin detection by magnetic resonance force microscopy, Nature (London) **430**, 329 (2004).

[19] O. Arcizet, V. Jacques, A. Siria, P. Poncharal, P. Vincent, and S. Seidelin, A single nitrogen-vacancy defect coupled to a nanomechanical oscillator, Nat. Phys. **7**, 879 (2011).

[20] S. Kolkowitz, A. C. Bleszynski Jayich, Q. P. Unterreithmeier, S. D. Bennett, P. Rabl, J. G. Harris, and M. D. Lukin, Coherent Sensing of a Mechanical Resonator with a Single-Spin Qubit, Science **335**, 1603 (2012).

[21] E. R. MacQuarrie, T. A. Gosavi, N. R. Jungwirth, S. A. Bhave, and G. D. Fuchs, Mechanical Spin Control of Nitrogen-Vacancy Centers in Diamond, Phys. Rev. Lett. **111**, 227602 (2013).

[22] P. Ovartchaiyapong, K. W. Lee, B. A. Myers, and A. C. Bleszynski Jayich, Dynamic strain-mediated coupling of a single diamond spin to a mechanical resonator, Nat.

Commun. **5**, 4429 (2014).
[23] A. Barfuss, J. Teissier, E. Neu, A. Nunnenkamp, and P. Maletinsky, Strong mechanical driving of a single electron spin, Nat. Phys. **11**, 820 (2015).
[24] D. A. Golter, T. Oo, M. Amezcua, K. A. Stewart, and H. Wang, Optomechanical Quantum Control of a Nitrogen-Vacancy Center in Diamond, Phys. Rev. Lett. **116**, 143602 (2016).
[25] S. Meesala, Y.-I. Sohn, H. A. Atikian, S. Kim, M. J. Burek, J. T. Choy, and M. Loncar, Enhanced Strain Coupling of Nitrogen-Vacancy Spins to Nanoscale Diamond Cantilevers, Phys. Rev. Appl. **5**, 034010 (2016).
[26] M. J. Burek, N. P. de Leon, B. J. Shields, B. J. M. Hausmann, Y. Chu, Q. Quan, A. S. Zibrov, H. Park, M. D. Lukin, and M. Loncar, Free-Standing Mechanical and Photonic Nanostructures in Single-Crystal Diamond, Nano Lett. **12**, 6084 (2012).
[27] B. Khanaliloo, H. Jayakumar, A. C. Hryciw, D. P. Lake, H. Kaviani, and P. E. Barclay, Single-Crystal Diamond Nanobeam Waveguide Optomechanics, Phys. Rev. X **5**, 041051 (2015).
[28] A. Sipahigil, R. E. Evans, D. D. Sukachev, M. J. Burek, J. Borregaard, M. K. Bhaskar, C. T. Nguyen, J. L. Pacheco, H. A. Atikian, C. Meuwly, R. M. Camacho, F. Jelezko, E. Bielejec, H. Park, M. Loncar, and M. D. Lukin, An integrated diamond nanophotonics platform for quantum-optical networks, Science **354**, 847 (2016).
[29] S. Mouradian, N. H. Wan, T. Schröder, and D. Englund, Rectangular photonic crystal nanobeam cavities in bulk diamond, Appl. Phys. Lett. **111**, 021103 (2017).
[30] J. P. Goss, R. Jones, S. J. Breuer, P. R. Briddon, and S. Öberg, The Twelve-Line 1.682 eV Luminescence Center in Diamond and the Vacancy-Silicon Complex, Phys. Rev. Lett. **77**, 3041 (1996).
[31] C. Hepp, T. Müller, V. Waselowski, J. N. Becker, B. Pingault, H. Sternschulte, D. Steinmüller-Nethl, A. Gali, J. R. Maze, M. Atatüre, and C. Becher, Electronic Structure of the Silicon Vacancy Color Center in Diamond, Phys. Rev. Lett. **112**, 036405 (2014).
[32] C. Hepp, Electronic Structure of the Silicon Vacancy Color Center in Diamond, Ph.D. thesis, University of Saarland (2014).
[33] L. J. Rogers, K. D. Jahnke, M. H. Metsch, A. Sipahigil, J. M. Binder, T. Teraji, H. Sumiya, J. Isoya, M. D. Lukin, P. Hemmer, and F. Jelezko, All-Optical Initialization, Readout, and Coherent Preparation of Single Silicon-Vacancy Spins in Diamond, Phys. Rev. Lett. **113**, 263602 (2014).
[34] J. N. Becker, J. Görlitz, C. Arend, M. Markham, and C. Becher, Ultrafast all-optical coherent control of single silicon vacancy colour centres in diamond, Nat. Commun. **7**, 13512 (2016).
[35] Y. Zhou, A. Rasmita, K. Li, Q. Xiong, I. Aharonovich, and W.-B. Gao, Coherent control of a strongly driven silicon vacancy optical transition in diamond, Nat. Commun. **8**, 14451 (2017).
[36] D. D. Sukachev, A. Sipahigil, C. T. Nguyen, M. K. Bhaskar, R. E. Evans, F. Jelezko, and M. D. Lukin, The silicon-vacancy spin qubit in diamond: quantum memory exceeding ten milliseconds and single-shot state readout, Phys. Rev. Lett. **119**, 223602 (2017).
[37] J. N. Becker and C. Becher, Coherence properties and quantum control of silicon vacancy color centers in diamond, Phys. Status Solidi A **214**, 1700586 (2017).
[38] J. J. Pla, K. Y. Tan, J. P. Dehollain, W. H. Lim, J. J. L. Morton, D. N. Jamieson, A. S. Dzurak, and A. Morello, A single-atom electron spin qubit in silicon, Nature **489**, 541 (2012).
[39] See Supplemental Material for additional details about the model and the state transfer protocols.
[40] Y.-I. Sohn, S. Meesala, B. Pingault, H. A. Atikian, J. Holzgrafe, M. Gundogan, C. Stavrakas, M. J. Stanley, A. Sipahigil, J. Choi, M. Zhang, J. L. Pacheco, J. Abraham, E. Bielejec, M. D. Lukin, M. Atatüre, and M. Loncar, Engineering a diamond spin-qubit with a nano-electromechanical system, arXiv:1706.03881.
[41] K. D. Jahnke, A. Sipahigil, J. M. Binder, M. W. Doherty, M. Metsch, L. J. Rogers, N. B. Manson, M. D. Lukin and F. Jelezko, Electron-phonon processes of the silicon-vacancy centre in diamond, New J. Phys. **17**, 043011 (2015).
[42] K. V. Kepesidis, M.-A. Lemonde, A. Norambuena, J. R. Maze, and P. Rabl, Cooling phonons with phonons: Acoustic reservoir engineering with silicon-vacancy centers in diamond, Phys. Rev. B **94**, 214115 (2016).
[43] P. Lodahl, S. Mahmoodian, and S. Stobbe, Interfacing single photons and single quantum dots with photonic nanostructures, Rev. Mod. Phys. **87**, 347 (2015).
[44] C. W. Gardiner and P. Zoller, *Quantum noise* (Springer, Berlin; New York, 2000).
[45] S. Massar and S. Popescu, Optimal extraction of information from finite quantum ensembles, Phys. Rev. Lett. **74**, 1259 (1995).
[46] M. Maldovan, Sound and heat revolutions in phononics, Nature (London) **503**, 209 (2013).
[47] J. I. Cirac, P. Zoller, H. J. Kimble, and H. Mabuchi, Quantum State Transfer and Entanglement Distribution among Distant Nodes in a Quantum Network, Phys. Rev. Lett. **78**, 3221 (1997).
[48] K. Jähne, B. Yurke, and U. Gavish, High-fidelity transfer of an arbitrary quantum state between harmonic oscillators, Phys. Rev. A **75**, 010301 (2007).
[49] A. N. Korotkov, Flying microwave qubits with nearly perfect transfer effciency, Phys. Rev. B **84**, 014510 (2011).
[50] U. Dorner and P. Zoller, Laser-driven atoms in half-cavities, Phys. Rev. A **66**, 023816 (2002).
[51] T. Schröder, M. E. Trusheim, M. Walsh, L. Li, J. Zheng, M. Schukraft, A. Sipahigil, R. E. Evans, D. D. Sukachev, C. T. Nguyen, J. L. Pacheco, R. M. Camacho, E. S. Bielejec, M. D. Lukin, and D. Englund, Scalable focused ion beam creation of nearly lifetime-limited single quantum emitters in diamond nanostructures, Nat. Commun. **8**, 15376 (2017).
[52] A. H. Safavi-Naeini and O. Painter, Proposal for an optomechanical traveling wave phononphoton translator, New J. Phys. **13**, 013017 (2011).
[53] R. N. Patel, Z. Wang, W. Jiang, C. J. Sarabalis, J. T. Hill, and A. H. Safavi-Naeini, A single-mode phononic wire, arXiv:1711.00847.
[54] C. Brendel, V. Peano, O. Painter, and F. Marquardt, Snowflake Topological Insulator for Sound Waves, arXiv:1701.06330.
[55] J. T. Shen and S. Fan, Coherent single photon transport in a one-dimensional waveguide coupled with superconducting quantum bits, Phys. Rev. Lett. **95**, 213001(2005).

[56] L. Zhou, H. Dong, Yu-xi Liu, C. P. Sun, and F. Nori, Quantum supercavity with atomic mirrors, Phys. Rev. A **78**, 063827 (2008).

[57] D. E. Chang, L. Jiang, A. V. Gorshkov, and H. J. Kimble, Cavity QED with atomic mirrors, New J. Phys. **14**, 063003 (2012).

[58] S. Meesala, Y-I. Sohn, *et al.*, Strain engineering of the silicon vacancy center in diamond, in preparation (2017).

[59] Ö. O. Soykal, R. Ruskov, and C. Tahan, Sound-Based Analogue of Cavity Quantum Electrodynamics in Silicon, Phys. Rev. Lett. **107**, 235502 (2011).

[60] R. Ruskov and C. Tahan, On-chip cavity quantum phonodynamics with an acceptor qubit in silicon, Phys. Rev. B **88**, 064308 (2013).

[61] T. Ramos, V. Sudhir, K. Stannigel, P. Zoller, and T. J. Kippenberg, Nonlinear Quantum Optomechanics via Individual Intrinsic Two-Level Defects, Phys. Rev. Lett. **110**, 193602 (2013).

[62] M. V. G. Dutt, L. Childress, L. Jiang, E. Togan, J. Maze, F. Jelezko, A. S. Zibrov, P. R. Hemmer, and M. D. Lukin, Quantum Register Based on Individual Electronic and Nuclear Spin Qubits in Diamond, Science **316**, 5829 (2007).

[63] A. Reiserer, N. Kalb, M. S. Blok, K. J. M. van Bemmelen, D. J. Twitchen, M. Markham, T. H. Taminiau, and R. Hanson, Robust quantum-network memory using decoherence-protected subspaces of nuclear spins, Phys. Rev. X **6**, 021040 (2016).